Heterobifunctional Rotaxanes for Asymmetric Catalysis

Noël Pairault, Hui Zhu,* Dennis Jansen, Alexander Huber, Constantin G. Daniliuc, Stefan Grimme, and Jochen Niemeyer*

In memory of Carsten Schmuck

Abstract: *Heterobifunctional rotaxanes serve as efficient catalysts for the addition of malonates to Michael acceptors. We report a series of four different heterobifunctional rotaxanes, featuring an amine-based thread and a chiral 1,1′-binaphthyl-phosphoric-acid-based macrocycle. High-level DFT calculations provided mechanistic insights and enabled rational catalyst improvements, leading to interlocked catalysts that surpass their non-interlocked counterparts in terms of reaction rates and stereoselectivities.*

Introduction

The mechanical bond[1] has emerged as a new design element for the generation of catalytically active species. The use of rotaxanes,[2] catenanes[3] or molecular knots[4] offers novel possibilities in catalysis, such as the development of switchable systems, the construction of highly congested reaction spaces or the linking of different functionalities via the mechanical bond.[5]

For an application in asymmetric catalysis, a number of chiral mechanically interlocked molecules (MIMs) have been developed.[6] In transition-metal catalysis, Leigh used rotaxanes with chiral diamine-based macrocycles for Ni-catalyzed enantioselective Michael additions,[7] while Goldup employed mechanically planar-chiral rotaxane ligands for Au-mediated cyclopropanations.[8] In the realm of organocatalysis, Leigh and Berna developed rotaxanes featuring nucleophilic secondary amines on the axle. Making use of either stereogenic

centers in close vicinity to the amine[9] or by employing the macrocycle to achieve a desymmetrization of a (pseudo)-symmetric thread,[10] these rotaxane catalysts were applied for enantioselective Michael additions or α-functionalizations.

In a slightly different approach, Takata developed chiral rotaxanes in which a catalytically active nucleophile (for example, a thiazole or pyridine) and a chiral BINOL-moiety are present on different subcomponents of the MIMs.[11] Nevertheless, the close vicinity of both components, brought about by the mechanical bond, allowed the use of these catalysts for enantioselective acylation reactions or in the benzoin condensation. Our group has recently reported the mechanical linking of two chiral 1,1′-binaphthyl-phosphoric acids in a [2]catenane.[12] The resulting bifunctional system showed drastically enhanced stereoselectivities in comparison to the non-interlocked monophosphoric acids in the transfer-hydrogenation of quinolines.[13]

Herein, we now report the first application of a chiral acid/base-functionalized rotaxane for asymmetric catalysis. We have combined a Brønsted-acidic macrocycle based on a chiral 1,1′-binaphthyl-phosphate unit with a Brønsted-basic thread featuring a central secondary amine. We envisaged that the cooperative action of both functional groups in asymmetric catalysis would be enhanced by the mechanical bond, thus leading to enhanced reaction rates and stereoselectivities. Indeed, using a combined experimental and theoretical approach, we were able to generate rotaxanated catalysts that show markedly increased reaction rates and stereoselectivities in comparison to their non-interlocked counterparts.

Results and Discussion

For the synthesis of the first-generation bifunctional chiral rotaxane (*S*)-**1a** (Scheme 1), we started by generating the macrocyclic 1,1′-binaphthyl-phosphoric acid (*S*)-**5a**.

This was performed by alkylation of (*S*)-**11a** with *O*-allyl-triethyleneglycol-tosylate, followed by ring-closing metathesis under dilute conditions (0.5 mM) to give the 38-membered macrocycle (*S*)-**13a**. Subsequent acid-induced MOM-deprotection and phosphorylation gave the desired macrocyclic phosphoric acid (*S*)-**5a** in good yield (36 % over four steps). All compounds were fully characterized by standard analytical methods (see the Supporting Information for details), in addition the macrocyclic diol **14a** could be analyzed by single-crystal X-ray analysis of a racemic sample.

Starting from macrocycle (*S*)-**5a**, we generated rotaxane (*S*)-**1a** in a passive-template approach. (*S*)-**5a** was mixed with the dialkynylated amine **21** to give the corresponding phos-

[*] Dr. N. Pairault, M. Sc. D. Jansen, A. Huber, Dr. J. Niemeyer
Institute of Organic Chemistry and
Center for Nanointegration Duisburg-Essen (CENIDE),
University of Duisburg-Essen
Universitätsstrasse 7, 45141 Essen (Germany)
E-mail: jochen.niemeyer@uni-due.de

Dr. H. Zhu, Prof. S. Grimme
Mulliken Center for Theoretical Chemistry,
Rheinische Friedrich-Wilhelms-Universität Bonn
Beringstrasse 4, 53115 Bonn (Germany)
E-mail: hui@thch.uni-bonn.de

Dr. C. Daniliuc
Institute of Organic Chemistry
Corrensstr. 40, 48149 Münster (Germany)
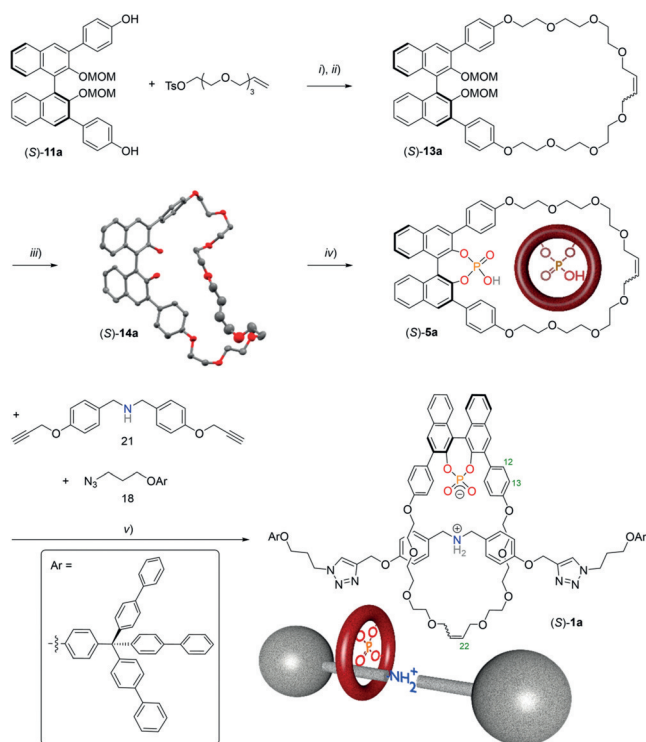
Scheme 1. Synthesis of rotaxane (*S*)-**1a**. i) (*S*)-**11a** (1 equiv), *O*-allyl-triethyleneglycol-tosylate (3 equiv), Cs$_2$CO$_3$, 80°C, CH$_3$CN; 70%; ii) Grubbs-II catalyst, CH$_2$Cl$_2$, 0.5 mM, 54%; iii) conc. HCl, 70°C, THF/MeOH, 99%; iv) POCl$_3$, pyridine, 60°C, then H$_2$O, 95%; v) (*S*)-**5a** (1 equiv), **21** (1.6 equiv), **18** (3.3 equiv), [Cu(MeCN)$_4$PF$_6$], CH$_2$Cl$_2$, 0°C, 33%. The structure of macrocycle (*S*)-**14a** in the solid state is shown (hydrogen atoms omitted for clarity and thermal ellipsoids set at the 60% probability level).[19]

phate–ammonium pseudorotaxane complex, which was stoppered with bulky azide **18** in the presence of Cu^I. To guarantee the isolation of pure zwitterionic NH$_2^+$/POO$^-$ [2]rotaxane, the compound was washed by acidic then neutral aqueous solution after silica gel column chromatography, yielding (*S*)-**1a** in 33% yield.

NMR analysis (Figure 1) reveals distinct chemical shift changes for the rotaxane (*S*)-**1a** in comparison to the macrocycle (*S*)-**5a**, the thread **3**, and the non-interlocked
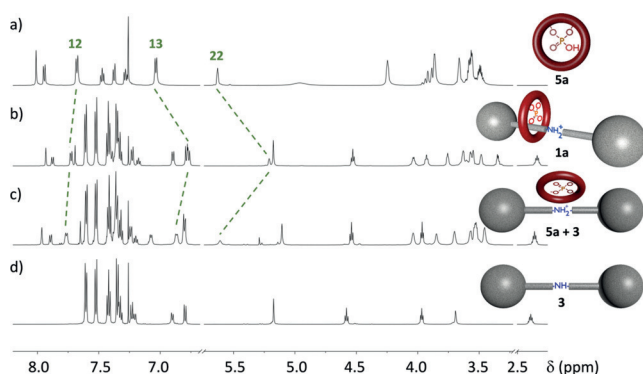

Figure 1. ^{1}H NMR spectra of a) macrocycle (*S*)-**5a**, b) rotaxane (*S*)-**1a**, c) 1:1 mixture of macrocycle (*S*)-**5a**, and d) thread **3** (all: 600 MHz, CDCl$_3$, 298 K, for numbering see Scheme 1).

mixture of (*S*)-**5a** with **3**. Finally, the interlocked nature of the rotaxane was unambiguously shown by MS/MS experiments, which show liberation of the thread upon fragmentation of the macrocycle (Supporting Information, Figures S23 and S24).

With the [2]rotaxane (*S*)-**1a** in hand, we set out to investigate its application in asymmetric catalysis. Based on the bifunctional phosphate–ammonium structure, we envisaged its use for the asymmetric Michael addition to α,β-unsaturated aldehydes. Such reactivity is known for non-interlocked phosphate–ammonium species (for example, the TRIP–morpholine pair).[14] The generally accepted mechanism involves iminium activation of the aldehyde by the nucleophilic amine, followed by stereoselective addition of the nucleophile to the chiral phosphate–iminium ion pair (thus termed as asymmetric counteranion-directed catalysis, ACDC).[15]

For our investigation, we employed the addition of diethyl malonate **8** to cinnamaldehyde **7a**, which yields the chiral Michael adduct **9a** (Table 1). Firstly, we employed the zwitterionic rotaxane (*S*)-**1a** as a catalyst, but almost no conversion was observed (less than 1% conversion after 7 days, see Figures S62–S104 in the Supporting Information for all conversion curves and chiral HPLC analyses). Assum-

Table 1: Catalytic results for rotaxane (*S*)-**1a** and its non-interlocked counterparts using different added bases (2 mol% catalyst, [D$_8$]THF, 25°C).[a]

Entry	Catalyst precursor	Added base MOH[b]	Conversion [%][c]	*ee* [%][d]
1	–	LiOH	<1	–
2	macrocyclic acid (*S*)-**5a**	LiOH	<1	–
3	thread **3**	–	10	–
4	rotaxane (*S*)-**1a**	–	<1	–
5	rotaxane (*S*)-**1a**	KOH	59	9
6	rotaxane (*S*)-**1a**	NaOH	83	16
7	rotaxane (*S*)-**1a**	LiOH	91	14
8	macrocyclic acid (*S*)-**5a** + thread **3**	KOH	8	0
9	macrocyclic acid (*S*)-**5a** + thread **3**	NaOH	9	5
10	macrocyclic acid (*S*)-**5a** + thread **3**	LiOH	45	22
11	acyclic acid (*S*)-**6a** + thread **3**	KOH	19	1
12	acyclic acid (*S*)-**6a** + thread **3**	NaOH	30	5
13	acyclic acid (*S*)-**6a** + thread **3**	LiOH	59	14

[a] [D$_8$]THF used as obtained (ca. 100 ppm H$_2$O). [b] Added as 1 M solution to THF solution of catalyst precursor, followed by drying in vacuo, prior to catalytic reaction. [c] Determined by ^{1}H NMR spectroscopy after 7 days. [d] Determined by chiral HPLC for isolated products.

ing that a strong phosphate–ammonium pairing would not allow ammonium deprotonation and thus block the reactivity of the amine, we generated the deprotonated rotaxane [(*S*)-**1a**]⁻M⁺ by addition of one equivalent of metal hydroxide MOH (M = K/Na/Li). Indeed, this gave catalytically active species, with the highest reaction rate observed in the case of LiOH (59 %/83 %/91 % conversion for KOH/NaOH/LiOH, respectively). Based on this, we could also demonstrate on/off/on switching of the catalyst by subsequent addition of LiOH/HCl/LiOH, respectively (Supporting Information, Figure S105). Significantly lower conversion was observed for the free thread **3** (used as the free amine R₂NH, 10 % conversion), and no conversion at all was found for LiOH only or for the macrocycle/LiOH combination. These controls clearly indicate that both metal–phosphate and amine are required for the catalytic activity.

Next, we investigated the influence of the mechanical bond on the catalytic behavior by using the non-interlocked mixture of macrocycle (*S*)-**5a** and thread **3** as well as the mixture of acyclic phosphoric acid (*S*)-**6a** (Table 1) and thread **3** as a comparison. For all three metal salts (KOH/ NaOH/LiOH), we consistently observed the lowest conversion for the macrocycle/thread pairs, while slightly higher conversions were observed for the acyclic phosphoric acid/ thread pairs. However, rotaxane (*S*)-**1a** was by far the most active catalyst in all cases, with reaction rates being 3.1–1.5 times higher in comparison to the acyclic phosphoric acid/ thread mixtures and even 9.2–2.0 times higher than those of the macrocycle/thread mixtures.

With respect to stereoselectivities, both the rotaxane (*S*)-**1a** and its non-interlocked counterparts only afforded low enantioselectivities (Table 1). However, three trends were observed: In case of Na/K, the rotaxane catalyst (*S*)-**1a** gave higher stereoselectivities (9 %/16 % *ee* for Na/K, respectively) than the non-interlocked catalysts (1 %/5 % and 0 %/5 % *ee* for Na/K, respectively). For the Li case, however, stereoselectivities for interlocked and non-interlocked species were comparable (14 %/22 %/14 % *ee* for (*S*)-**1a** / (*S*)-**5a** + **3** / (*S*)-**6a** + **3**, respectively). Variation of the solvent (CD₂Cl₂, [D₈]toluene or [D₆]DMSO) led to unchanged or decreased stereoselectivities (Supporting Information, Table S1).

To our knowledge, the phosphate–ammonium-catalyzed Michael addition has not yet been investigated theoretically.[16] We set out to explore the structures of rate- and stereo-determining intermediates and to rationalize the experimentally observed trends in reaction rates and stereoselectivities based on high-level density function theory (DFT) calculations. Our well established state-of-the-art DFT protocol (at the PW6B95-D3/def2-QZVP + COSMO-RS// TPSS-D3/ def2-TZVP + COSMO level[17] in THF solution) was applied, and the final Gibbs free energies (at 298 K and 1 M reference concentration) are used in our discussion. The initial structures and reaction paths were explored with the efficient GFN-xTB method.[17]

Our DFT calculations (Figure 2) show that the stoichiometric reaction between the non-interlocked model precatalyst **S⁻NmhH⁺** (phosphate–ammonium pair) and the strong base **Liw₂OH** (Li(H₂O)₂OH) is highly exergonic by −25.0 kcal mol⁻¹ to form the lithium-phosphate complex **SLiw₂** with two coordinated water molecules as well as the free amine base **Nmh** (or NMe₂H) in THF solution. The substrate **Meh** (malonate) binds through two ester groups to the lithium site of **SLiw₂** to replace one H₂O ligand, leading to a more C−H acidic malonate from which a proton can be transferred to the free amine base **Nmh**. This proton-transfer reaction is only 1.0 kcal mol⁻¹ endergonic over a low barrier of 8.4 kcal mol⁻¹ thus may reversibly lead to the ammonium phosphate **S⁻NmhH⁺** along with the lithium-activated malonate **MeLiw** as potential Michael donor. At this point, at least two pathways of Michael addition to cinnamaldehyde **Pho** (cinnamaldehyde) are possible depending on if the asymmetric phosphate anion **S⁻** is involved.

In the first path, direct Michael addition between **MeLiw** and **Pho** occurs via the transition structure **MeLiwPho_ts**, which is 22.1 kcal mol⁻¹ endergonic over a barrier of 23.5 kcal mol⁻¹ to form the zwitterionic adduct **MeLiwPho** (not shown in Figure 2), where the enolate-type addition product is bound to the Li-water cluster. In the presence of **S⁻NmhH⁺**, the adduct **MeLiwPho** can be stabilized by the binding of phosphate anion **S** to Li, followed by facile proton transfer (via **SLiwMePhon_ts**) from **NmhH⁺** to the enolate α-carbon, eventually leading to the final Michael-addition product **MePhho** and regenerated **SLiw₂** and **Nmh** as actual catalyst.

Such direct Michael addition of free **MeLiw** may occur equally at both sides of the **Pho** substrate, eventually leading to racemic final adduct **MePhho** with an overall barrier of 24.5 kcal mol⁻¹ (difference between **MeLiwPho_ts** and **SLiw-Meh** + **Nmh**).

Alternatively, the (*S*)-symmetric phosphate anion **S⁻** may bind to the lithium site of **MeLiw** to form the unstable complex **SLiwMe⁻** before the nucleophilic addition to the **Pho** substrate, which may lead to the desired stereoselectivity. Further to the strong O–Li coordination bond, **S⁻** may bind to **MeLiw** in two configurations either with or without an additional O···HO hydrogen bond to the Li-bound H₂O ligand. In presence of the hydrogen bond, the reaction is kinetically favored by 0.7 kcal mol⁻¹ and leads to preferred formation of the (*S*)-product, (*S*)-**MePhho**, with an enantioselectivity of 1.4 kcal mol⁻¹. In contrast, the (*R*)-product is favored by 0.7 kcal mol⁻¹ in the absence of the additional hydrogen bond. Yet, this phosphate-directed (*S*)-selective channel via **SLiwMe⁻Pho_tsS** is still kinetically slightly less favorable (barrier of 24.8 kcal mol⁻¹, difference between **SLiwMe⁻Pho_tsS** and **SLiwMeh** + **Nmh**) than the direct but racemic Michael addition.

To take into account the rotaxanation in our calculations, we mimicked the high local concentration of functional groups in the interlocked structure by assuming an interaction between the amine/ammonium-thread and the Li-phosphate species (complexes **SLiwMenPho_tsR** and **SLiwNmh,** shown in red in Figure 2). Such interaction results in a reduction of the overall barrier by about 0.8 kcal mol⁻¹ for the pathway involving the ammonium-cation **Men** (barrier of 23.7 kcal mol⁻¹). This shows that for the interlocked catalyst, the reaction is kinetically competitive over the racemic pathway, although stereoselectivity for this pathway is small: the (*R*)-product favored by 0.7 kcal mol⁻¹ (see the Supporting Information).
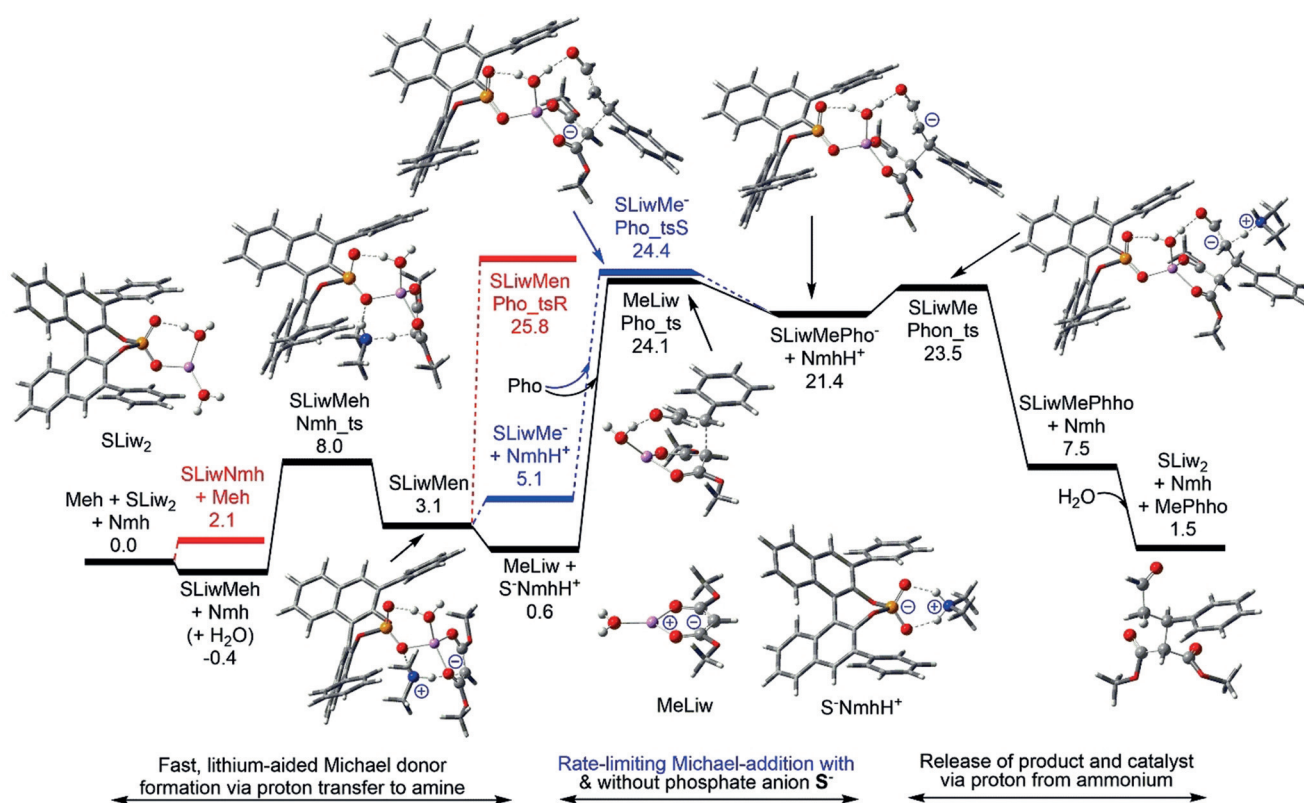
Figure 2. DFT-computed reaction free energy paths (in kcal mol^{-1}, at 298 K, 1 M reference concentration) for the catalytic Michael addition of model systems of dimethylmalonate **Meh** and cinnamaldehyde **Pho** (PhCH=CHCHO) using the acyclic lithium (S)-1,1′-biphenyl-phosphate **SLiw$_2$** and dimethylamine **Nmh** (NMe$_2$H) as catalyst, formed from the exergonic reaction of the ammonium phosphate salt pre-catalyst **S$^-$NmhH$^+$** and the strong base **Liw$_2$OH** (Li(H$_2$O)$_2$OH). The rotaxane catalyst is mimicked by assuming an interaction of the amine/ammonium-thread and the Li-phosphate species (shown in red). Crucial P, O, N, C, and H atoms are highlighted as violet, red, blue, gray, and white balls, respectively, along with gray carbon backbones, and most hydrogen atoms are omitted for clarity.

In summary, our DFT-computed mechanism is consistent with the observed catalytic role of amine, metal ions, and phosphate anion, with small stereoselectivities observed mainly due to two reasons: 1) competing binding configurations between **S$^-$** and the Michael donor **MeLiw**; 2) lower **S$^-$** affinity of **MeLiw** than **NmhH$^+$**. Note that the generally accepted mechanism of ACDC-type Michael addition via the anion-bound iminium as key intermediate (instead of **SLiwMe$^-$**) was also considered in our DFT calculations but it encounters a much higher and chemically unrealistic barrier of about 35 kcal mol^{-1} for the **SLiw$_2$**-catalyzed iminium formation in the present case (Supporting Information, Figure S106).

According to the DFT-computed mechanism, the stereoselectivity of the addition reaction could be enhanced by introducing bulky substituents near the oxygen binding sites of **S$^-$** that may favor single-mode **MeLiw** binding with enhanced affinity via stronger dispersion interactions. Such a modified phosphate anion **Sb$^-$**, featuring bulky ^{i}Pr groups in the 3,5-positions, shows a 3.5 kcal mol^{-1} higher affinity to the malonate substrate **Meh** as well as an enhanced stereoselectivity (1.9 kcal mol^{-1} in favor of the (S)-product) for the asymmetric Michael addition.

Based on these conclusions, we performed an evolution of the rotaxane structure (S)-**1a** and synthesized three variants.

Further to introduction of bulky isopropyl groups in the 3,5-positions (as suggested by DFT), we also designed a shorter thread in order to enhance the proximity between the relevant functional groups (phosphate and amine). The synthesis of the novel ^{i}Pr$_2$-substituted macrocycle (S)-**5b** and the novel rotaxanes (S)-**2a** (shorter thread only) and (S)-**1b/2b** (^{i}Pr$_2$-macrocycle with long/short thread, respectively) was performed in close analogy to the synthesis of (S)-**1a** (see above), giving three additional rotaxanes in 28–58% yield (Scheme 2; see the Supporting Information for details and full characterization).

(S)-**1a** (for n = 1 ; R = H)
(S)-**2a** (for n = 0 ; R = H)
(S)-**1b** (for n = 1 ; R = ^{i}Pr)
(S)-**2b** (for n = 0 ; R = ^{i}Pr)
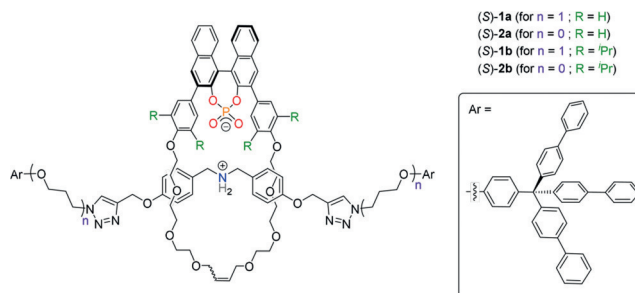
Scheme 2. Structures of [2]rotaxanes (S)-**1a**, (S)-**2a**, (S)-**1b**, and (S)-**2b**.
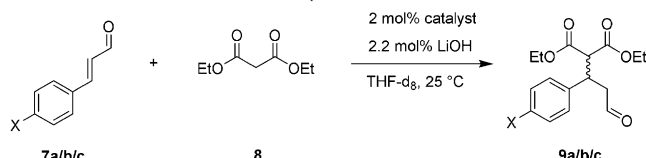
Using the optimized reaction conditions (2 mol% catalyst, 2.2 mol% LiOH, [D$_8$]THF, RT), we investigated the catalytic activity and stereoselectivity of rotaxanes (S)-**1a/2a/1b/2b** in comparison to the respective non-interlocked mixtures of macrocycle and thread (Table 2).[18] Catalysts **1a**

Table 2: Catalytic results for different rotaxane catalysts **1a/2a/1b/2b** and their non-interlocked counterparts.

Entry	Catalyst precursor	Aldehyde substituent X	Conversion [%][a]	*ee* [%][b]
1	rotaxane (S)-**1a**	H	91	14
2	macrocyclic acid (S)-**5a** + thread **3**	H	45	22
3	rotaxane (S)-**2a**	H	92	14
4	macrocyclic acid (S)-**5a** + thread **4**	H	35	23
5	rotaxane (S)-**1b**	H	88	53
6	macrocyclic acid (S)-**5b** + thread **3**	H	76	9
7	rotaxane (S)-**2b**	H	87	37
8	macrocyclic acid (S)-**5b** + thread **4**	H	78	7
9	rotaxane (S)-**1b**	OMe	54	44
10	macrocyclic acid (S)-**5b** + thread **3**	OMe	40	16
11	rotaxane (S)-**1b**	NO$_2$	92	49
12	macrocyclic acid (S)-**5b** + thread **3**	NO$_2$	56	14

[a] Determined by ^{1}H NMR spectroscopy after 7 days. [b] Determined by chiral HPLC for isolated products.

and **2a**, which differ in the length of the thread, show no noticeable differences with regard to rate or stereoselectivity (91/92% conversion after 7 days, 14/14% *ee*, respectively), and the same is true for their non-interlocked counterparts (45/35% conversion, 22/23% *ee*, respectively).

In stark contrast to this, the ^{i}Pr$_2$-substituted rotaxanes **1b/2b** give significantly higher stereoinduction without lowering the reaction rates (88/87% conversion, 53/37% *ee*, respectively), while their non-interlocked counterparts are slightly slower and significantly less stereoselective (76/78% conversion, 9/7% *ee*, respectively). The same trend can be observed upon variation of the substrate by using differently substituted Michael acceptors **7b/c**, featuring *p*-OMe/*p*-NO$_2$ substituents, respectively, which show moderate stereoselectivity in case of rotaxane **1b** (44/49% *ee*, respectively), but poor stereoselectivity for the non-interlocked catalyst (16/14% *ee*, respectively).

Despite these clear trends and the enhanced stereoselectivities for the rotaxane catalysts, we were wondering why the absolute stereoselectivity remains moderate. Based on DFT-calculations, it seems that the racemic Michael addition between free **MeLiw** and **Pho** still remains kinetically competitive over nearly the same barrier as the channel

involving the chiral phosphate, even in the new catalyst design. We will address this fact in due course by further modification of the rotaxane structures.

Conclusion

In summary, we could show that the mechanical bond can indeed serve as an efficient tool for the modification and improvement of organocatalysts. The mechanical linking leads to a significant increase in reaction rates for all cases investigated here, which can be attributed to the high local concentrations of the functional groups in the [2]rotaxane catalyst. In terms of stereoselectivity, we established that the length of the thread has no significant influence, while the exact substitution pattern of the macrocycle has a major impact. Introduction of bulky ^{i}Pr groups led to a significant increase in stereoselectivity, however only in case of the mechanically interlocked catalysts. This finding may well pave the route for the generation of more selective interlocked catalysts for such organocatalytic transformations that have failed to be realized with high stereoselectivities up to date.

Acknowledgements

Conflict of interest

The authors declare no conflict of interest.

[1] J. F. Stoddart, *Chem. Soc. Rev.* **2009**, *38*, 1802–1820.

[2] M. Xue, Y. Yang, X. Chi, X. Yan, F. Huang, *Chem. Rev.* **2015**, *115*, 7398–7501.

[3] G. Gil-Ramírez, D. A. Leigh, A. J. Stephens, *Angew. Chem. Int. Ed.* **2015**, *54*, 6110–6150; *Angew. Chem.* **2015**, *127*, 6208–6249.

[4] S. D. P. Fielden, D. A. Leigh, S. L. Woltering, *Angew. Chem. Int. Ed.* **2017**, *56*, 11166–11194; *Angew. Chem.* **2017**, *129*, 11318–11347.

[5] a) D. Sluysmans, J. F. Stoddart, *Trends Chem.* **2019**, *1*, 185–197; b) J. E. Lewis, M. Galli, S. M. Goldup, *Chem. Commun.* **2016**, *52*, 298–312; c) V. Blanco, D. A. Leigh, V. Marcos, *Chem. Soc. Rev.* **2015**, *44*, 5341–5370; d) E. A. Neal, S. M. Goldup, *Chem.*

Commun. **2014**, *50*, 5128–5142; e) D. A. Leigh, V. Marcos, M. R. Wilson, *ACS Catal.* **2014**, *4*, 4490–4497.

[6] a) E. M. G. Jamieson, F. Modicom, S. M. Goldup, *Chem. Soc. Rev.* **2018**, *47*, 5266–5311; b) N. H. Evans, *Chem. Eur. J.* **2018**, *24*, 3101–3112; c) N. Pairault, J. Niemeyer, *Synlett* **2018**, *29*, 689–698.

[7] S. Hoekman, M. O. Kitching, D. A. Leigh, M. Papmeyer, D. Roke, *J. Am. Chem. Soc.* **2015**, *137*, 7656–7659.

[8] A. W. Heard, S. M. Goldup, *ChemRxiv* **2019**, https://doi.org/10.26434/chemrxiv.9701789.v1.

[9] a) A. Martinez-Cuezva, M. Marin-Luna, D. A. Alonso, D. Ros-Ñiguez, M. Alajarin, J. Berna, *Org. Lett.* **2019**, *21*, 5192–5196; b) V. Blanco, D. A. Leigh, V. Marcos, J. A. Morales-Serna, A. L. Nussbaumer, *J. Am. Chem. Soc.* **2014**, *136*, 4905–4908.

[10] a) M. Dommaschk, J. Echavarren, D. A. Leigh, V. Marcos, T. A. Singleton, *Angew. Chem. Int. Ed.* **2019**, *58*, 14955–14958; b) Y. Cakmak, S. Erbas-Cakmak, D. A. Leigh, *J. Am. Chem. Soc.* **2016**, *138*, 1749–1751.

[11] a) K. Xu, K. Nakazono, T. Takata, *Chem. Lett.* **2016**, *45*, 1274–1276; b) Y. Tachibana, N. Kihara, T. Takata, *J. Am. Chem. Soc.* **2004**, *126*, 3438–3439; c) Y. Tachibana, N. Kihara, K. Nakazono, T. Takata, *Phosphorus Sulfur Silicon Relat. Elem.* **2010**, *185*, 1182–1205.

[12] R. Mitra, M. Thiele, F. Octa-Smolin, M. C. Letzel, J. Niemeyer, *Chem. Commun.* **2016**, *52*, 5977–5980.

[13] R. Mitra, H. Zhu, S. Grimme, J. Niemeyer, *Angew. Chem. Int. Ed.* **2017**, *56*, 11456–11459; *Angew. Chem.* **2017**, *129*, 11614–11617.

[14] S. Mayer, B. List, *Angew. Chem. Int. Ed.* **2006**, *45*, 4193–4195; *Angew. Chem.* **2006**, *118*, 4299–4301.

[15] a) E. P. Ávila, G. W. Amarante, *ChemCatChem* **2012**, *4*, 1713–1721; b) M. Mahlau, B. List, *Isr. J. Chem.* **2012**, *52*, 630–638; c) M. Mahlau, B. List, *Angew. Chem. Int. Ed.* **2013**, *52*, 518–533; *Angew. Chem.* **2013**, *125*, 540–556.

[16] a) H. G. O. Alvim, D. L. J. Pinheiro, V. H. Carvalho-Silva, M. Fioramonte, F. C. Gozzo, W. A. da Silva, G. W. Amarante, B. A. D. Neto, *J. Org. Chem.* **2018**, *83*, 12143–12153; b) F. Duarte, R. S. Paton, *J. Am. Chem. Soc.* **2017**, *139*, 8886–8896;

c) Z. Kang, Y. Wang, D. Zhang, R. Wu, X. Xu, W. Hu, Z. Kang, W. Hu, *J. Am. Chem. Soc.* **2019**, *141*, 1473–1478; d) T. J. Seguin, S. E. Wheeler, *Angew. Chem. Int. Ed.* **2016**, *55*, 15889–15893; *Angew. Chem.* **2016**, *128*, 16121–16125.

[17] a) F. Eckert, A. Klamt, *AIChE J.* **2002**, *48*, 369–385; b) P. Deglmann, K. May, F. Furche, R. Ahlrichs, *Chem. Phys. Lett.* **2004**, *384*, 103–107; c) F. Eckert, A. Klamt, **2015**, *COSMOtherm*, Version C3.0, Release 16.01; COSMOlogic GmbH & Co. KG, Leverkusen, Germany; d) S. Grimme, *Chem. Eur. J.* **2012**, *18*, 9955–9964; e) S. Grimme, H. Kruse, L. Goerigk, G. Erker, *Angew. Chem. Int. Ed.* **2010**, *49*, 1402–1405; *Angew. Chem.* **2010**, *122*, 1444–1447; f) S. Grimme, S. Ehrlich, L. Goerigk, *J. Comput. Chem.* **2011**, *32*, 1456–1465; g) A. Klamt, G. Schüürmann, *J. Chem. Soc. Perkin Trans. 2* **1993**, 799–805; h) J. Tao, J. P. Perdew, V. N. Staroverov, G. E. Scuseria, *Phys. Rev. Lett.* **2003**, *91*, 146401; i) F. Weigend, *Phys. Chem. Chem. Phys.* **2006**, *8*, 1057–1065; j) F. Weigend, R. Ahlrichs, *Phys. Chem. Chem. Phys.* **2005**, *7*, 3297–3305; k) F. Weigend, F. Furche, R. Ahlrichs, *J. Chem. Phys.* **2003**, *119*, 12753–12762; l) F. Weigend, M. Häser, H. Patzelt, R. Ahlrichs, *Chem. Phys. Lett.* **1998**, *294*, 143–152; m) Y. Zhao, D. G. Truhlar, *J. Phys. Chem. A* **2005**, *109*, 5656–5667; n) *TURBOMOLE V7.3*, **2018**, a development of University of Karlsruhe and Forschungszentrum Karlsruhe GmbH, 1989–2007, TURBOMOLE GmbH, since 2007; available from http://www.turbomole.com; o) S. Grimme, C. Bannwarth, P. Shushkov, *J. Chem. Theory Comput.* **2017**, *13*, 1989–2009.

[18] No further comparison with the combination of acyclic phosphoric acids + threads was conducted since these did not differ in stereoselectivity in the initial investigation using rotaxane **1a**.

[19] CCDC 1954621 contains the supplementary crystallographic data for this paper. These data are provided free of charge by The Cambridge Crystallographic Data Centre.